IEEE Photonics Journal
An IEEE Photonics Society Publication

Open Access

A Sub-λ-Size Modulator Beyond the Efficiency-Loss Limit

Volume 5, Number 4, August 2013

Chen Huang
Rory J. Lamond
Sarah K. Pickus
Zhuo Ran Li
Volker J. Sorger

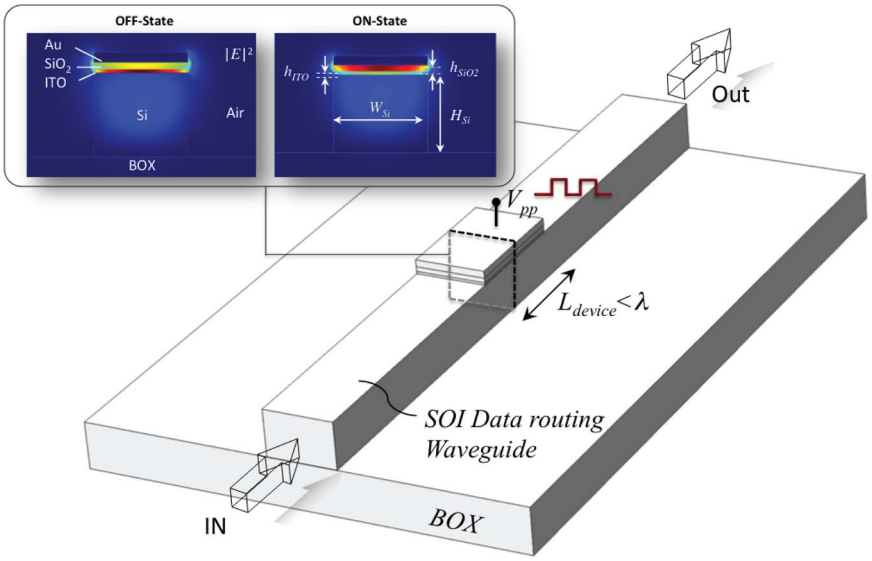

DOI: 10.1109/JPHOT.2013.2274772
1943-0655

IEEE photonics SOCIETY

IEEE

A Sub-λ-Size Modulator Beyond the Efficiency-Loss Limit

Chen Huang, Rory J. Lamond, Sarah K. Pickus, Zhuo Ran Li, and Volker J. Sorger

Department of Electrical and Computer Engineering, School of Engineering and Applied Science, The George Washington University, Washington, DC 20052 USA

DOI: 10.1109/JPHOT.2013.2274772

Manuscript received June 29, 2013; revised July 11, 2013; accepted July 12, 2013. Date of publication July 25, 2013; date of current version August 7, 2013. This work was supported under funds from the School of Engineering and Applied Science, The George Washington University. Corresponding author: V. Sorger (e-mail: sorger@gwu.edu).

Abstract: Electrooptic modulators (EOMs) are key devices in performing the conversion between the electrical and optical domains in data communication links. With respect to a road map for photonic computing, future EOMs are required to be highly scalable, should feature strong modulation performance, and must not consume much power during operation. In light of these requirements, here, we investigate indium–tin–oxide (ITO) as an electrooptic switching material. The results show that ITO is capable of changing its extinction coefficient by a factor of 136. Utilizing these findings, we analyze an ultracompact (i.e., sub-λ long $\lambda = 1310$ nm) electroabsorption modulator based on a plasmonic MOS-mode design. In our analysis, we investigate the performance, i.e., the extinction ratio and insertion loss of the device as a function of various geometric parameters of the device. The optimized device is 0.78 λ long and features an extinction ratio and on-chip insertion loss of about 6 dB/μm and 0.7 dB, respectively. Furthermore, we suggest a metric to benchmark electroabsorption modulators and show that silicon plasmonics has potential for high-end switching nodes in future integrated photonic circuits.

Index Terms: Silicon nanophotonics, plasmonics optoelectronic materials, nonlinear integrated optics, waveguide devices.

1. Introduction

Continued advancement of modern ICs is challenged in multiple ways. A limiting factor for on-board and on-chip systems is the I/O bandwidth, while for intra-chip the capacitive delay of the metal interconnects is becoming more severe with every scaling node [1]. For data communication, the bosonic nature of photons has been utilized to provide enormous data bandwidth in fiber networks. With this success the case for photonic integration was made [2], [3]. The electro-optic (EO) conversion of transmitters takes place in electro-optic modulators (EOM), which allow for controlling the amplitude, phase, and polarization of an optical beam electrically. The widely used mechanisms for optical modulation are 2nd and 3rd order optical non-linear effects, i.e., Pockel's, Kerr, and QCSE, and free carrier dispersive effects [4], [5]. For instance the Intel team demonstrated an optical phase modulation based on a metal–oxide–semiconductor (MOS) capacitor structure embedded in a silicon waveguide [5]. However, sizeable device footprints resulting in large insertion losses are required for achieving the expected modulation depth owing to weak light-matter-interactions [5]. This weak EO modulation can, in general, be enhanced by deploying high-quality (Q) factor cavities [6]. However, these architectures are somewhat impractical for on-chip designs due to narrow spectral bandwidths, small fabrication and operation

(i.e., temperature) tolerance, and long photon lifetimes, which limit modulation bandwidth to the few to ten's of GHz range for cavity Q's in the 10-100 k range, respectively. Emerging materials with high-modulation capability have been proposed and demonstrated for EO applications [5], [7]–[9]. For instance the Fermi-level of Graphene, placed on a Silicon-on-Insulator (SOI) waveguide, can be tuned in and out of resonance with the operating photon energy via an electrical bias [5], [9]. While higher modulation efficiency than simply modulating the carrier density inside a Silicon waveguide was achieved in this Graphene/Silicon device, its footprint of tens of micrometer and relatively high voltages were required due to the weak interaction of the nanometer thin Graphene layer with the optical mode [5]. Recently the plasmonic (i.e., metal-optics) field enhancement has been proposed [10], [11] and demonstrated to enhance the electro-optic modulation strength, i.e., extinction ratio [8], [12]. However, the field enhancement that increases the extinction ratio often introduces undesired effects, such as very high optical losses due to the influence of the metal deployed to confine the optical mode [12]. While a reasonably high performing plasmonic-photonic hybrid EOM was demonstrated [8], the detailed design-of-experiment (DOE) is still outstanding for hybrid devices.

Here, we provide a benchmarking framework for various material systems of electro-absorption modulators and show that plasmonic devices clearly outperform classical approaches. Furthermore, we present the design of a plasmonic EOM device based on refractive index data of a novel active EO material—Indium-tin-oxide (ITO). This analysis investigates an ultra-compact (i.e., sub-λ long), electro-absorption modulator based on a plasmonic MOS-mode design. The active layer consisting of ITO is strategically inserted into the high field MOS capacitor gap for optimized modal overlap. In our analysis, we investigate the performance, i.e., the extinction ratio (ER) and insertion loss (IL) of the device as a function of various geometric device parameters. The optimized device features an ER and IL of close to 6 dB/μm and 0.7 dB, respectively, and is only 0.78λ long. Note, this EO switching node can be arbitrarily placed onto a Silicon-on-Insulator passive waveguide routing platform toward compact and high-performance hybrid opto-electronic circuits.

2. Benchmarking Electro-Absorption Modulators

Since an EOM's function is to encode electrical data into the optical domain, the modulation efficiency and the bandwidth (i.e., speed) of the device are key performance figures. The slope efficiency of modulation, η_{mod}, is the ratio of the extinction ratio, divided by the applied peak-to-peak Voltage V_{pp}

$$ER = \frac{P_{out}(V_b = V_{OFF})}{P_{out}(V_b = V_{ON})} = \frac{T(L, \Delta\alpha)}{T_0} \Rightarrow \eta_{\mathrm{mod}} = \frac{ER}{V_{pp}} \tag{1}$$

where $V_{pp} = V_{ON} - V_{OFF}$. Here, "ON" and "OFF" relate to the device state, not to the actual voltage level, i.e., one of the two voltage states does not necessarily have to be zero. Typically V_{ON} is biased to a specific voltage to satisfy a particular device or circuit design goal (e.g., high ER, symmetric signal, linear device response, etc). The induced loss change is given via $\Delta\alpha = 4\pi\Delta\kappa/\lambda$ and with Beer's law the attenuation as a function modulator device length via $T(L, \Delta\alpha) = T_0 exp(-\Delta\alpha L)$, where T is the transmitted signal, λ is the operation wavelength, κ the imaginary part of the complex refractive index, $\tilde{n} = n + i\kappa$, and α the incurred loss over the device length, L. This equation set illustrates that a stronger $\Delta\kappa$ is intimately linked with higher an ER (note conversion to dB scale not shown, since trivial). With novel EOM device designs emerging, it is imperative and helpful to define a metric or figure-of-merit (FOM) that encompass those novel architectures. The classical FOM for EOM device demonstrations is given by

$$(FOM)_{Device} = \frac{ER}{V_{pp}} \cdot f_{3dB}. \tag{2}$$

This definition is logical, since it encompasses the modulation strength (i.e., ER), the modulation efficiency (i.e., ER/V_{pp}), and the modulation speed, f_{3dB}. A recent analysis on electro-refractive

(EO) modulators by Lin *et al.* [13] has shown the fundamental tradeoffs between EO modulation 3 dB-bandwidth and its subsequent energy requirement, i.e., Energy/bit; they share a square relation given by $E/bit = 1/2K(V_{pp})f_{3dB}^2$, where K is a bias-dependent constant contingent on the EO index modulation mechanism, material parameters and device geometry [13]. Interestingly, the aforementioned approach in deploying high Q-cavities to enhance the EO modulation efficiency is actually limiting the achievable bandwidth due to parasitic long photon lifetimes. For example, a device with a Q of 40 000 [6] results in modulation speeds of 25.7 GHz at telecom frequencies—clearly a limitation to ever increasing channel speeds. Thus, the aim is to either utilize low-Q EOM designs or refrain from a cavity altogether—at least from a bandwidth point of view. However, without the light-matter-interaction enhancement of the cavity, the modulation efficiency can be compromised. A possible solution benign to the low-Q approach is given by metal-based photonic devices; for instance, surface plasmons [14], collective electron oscillations on metal-dielectric interfaces, have shown to strongly enhance optical non-linear effects, such as EO modulation [8], [12]. Interestingly, such strong EO effect enhancement counterweights the high propagation losses classically associated with plasmonic devices. Thus, high-performance devices with λ-size footprints should be feasible, as we show below.

However, while the case for plasmonic devices for modulation and switching has been made [9]–[11], many emerging demonstrations do not report on high-speed bandwidth measurements. Thus, Eqn. (2) does not provide a sufficient benchmarking guidance at this early stage of emerging device architectures. Here, we propose an alternative metric, more suitable for capturing the performance of emerging EOM devices. We term it "physical" FOM since it relates device performance to typical computed values from simulation results

$$FOM_{Physical} = \frac{\Delta\tilde{n}_{eff}(V_{pp})}{V_{pp}\cdot\mu\mathrm{m}}\cdot\left(\frac{1}{IL}\right)_{on-chip,V=Von} \tag{3}$$

where Δn_{eff} is the ER substituting effective index as a function of voltage bias, which can be Δn or $\Delta\kappa$ for phase modulating devices, or electro-absorption modulators, respectively. Furthermore, $\Delta n_{eff}/V_{pp}$ captures the modulation efficiency. Since the optical on-chip power levels are critical to designing reliable photonic circuits the insertion loss (IL) defined by Eq. (4) should be taken into account, since it adds the power penalty into the device design picture. That is, for future high-performing photonic links, increasing power constrains are becoming "hard" design criteria especially on the device level [15]

$$IL = \frac{P_{in} - P_{out}(V_b = V_{ON})}{P_{in}} = 1 - \frac{T(L,\alpha_{ON})}{T_0} = 1 - exp(-\alpha_{ON}L) = 1 - exp\left(-\frac{4\pi\kappa_{ON}}{\lambda}L\right). \tag{4}$$

Notice that we have not taken care of the modulation bandwidth yet. Assuming the device internal modulation mechanism is faster than the capacitive delay, the following approximation can be made: $f_{3dB} = 1/RC$, where R is the resistance and C is the device capacitance, and C scaling with length, the bandwidth of the device scales inversely proportional to length. With plasmonic emerging devices pushing for (sub)micron-long device lengths, we here suggest to normalize the physical FOM by $1/\mu$m to capture the speed potential of emerging design proposals.

Deploying this physical FOM [Eq. (3) and (4)] on a variety of material platforms we arrive at Fig. 1. To enhance differentiation, we choose to categorize devices by the type of active material and substrate platform (colors), and emerging concepts and/or materials such as plasmonic, Graphene, VO_2, ITO (open symbols). The performance sweet spot is found in the upper right corner where the dashed line is pointing. The latter can be viewed as a technology progression of device advancements. These results show a cluster effect in the lower left corner for traditional (i.e., diffraction limited) device architectures, which extends to the lower right corner as improvements on losses have been made in recent years. However, only minor improvements on the modulation efficiency have been made (see the vertical axis in Fig. 1).

Highlighting an empirical region of diffraction-limited device performance (gray shading Fig. 1), the device design trade-off between modulation efficiency and optical losses become apparent, i.e.,

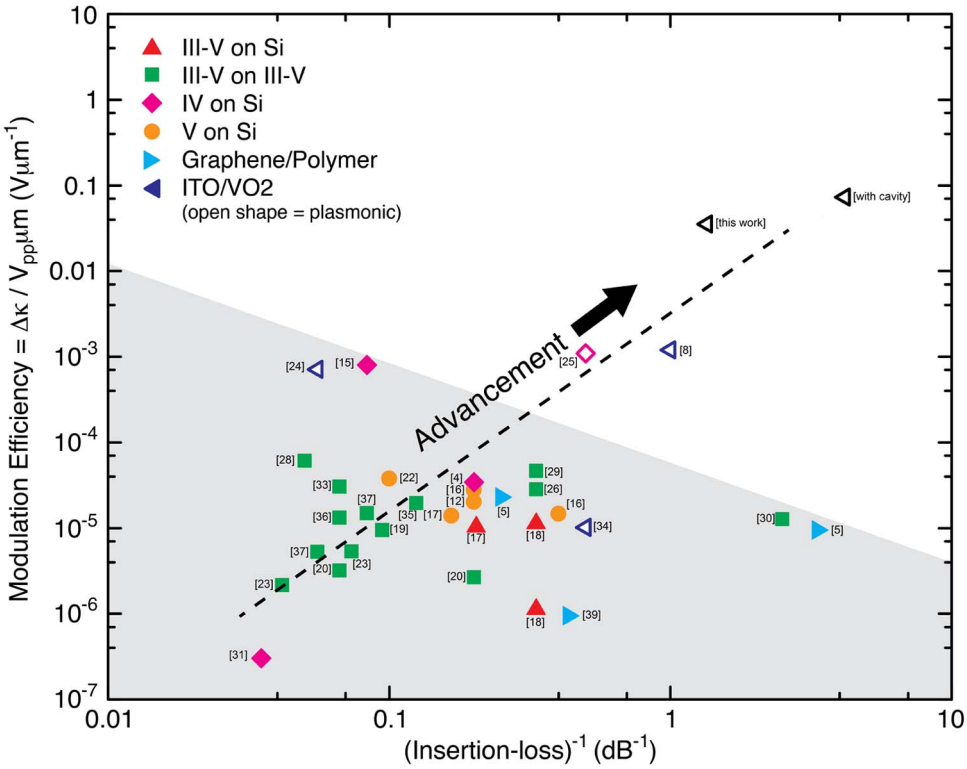

Fig. 1. Figure-of-Merit for EO modulators is based on modulation efficiency ($ER/\mu m V_{pp}$), which incorporates the obtainable modulation bandwidth (see text), and power penalty (i.e., insertion loss). The gray-shaded area denotes an empirical performance limitation of diffraction-limited device designs. Plasmonic devices (open shapes) and emerging active switching materials allow surpassing this shortcoming and contribute to the advancement of this technology. A low Q-cavity can enhance our analyzed devices performance with details to be reported elsewhere.

sloping to the lower right corner. This trend is not unexpected and showcases the challenge of designing a device featuring strong light-matter-interactions and minimized on-chip insertion losses simultaneously. Interestingly, even in the unpractical limit of infinite-high insertion loss, the diffraction-limited devices show limited modulation efficiencies saturating around 0.01 V/μm-dB. The reason for this originates from the weak modal index change, $\Delta n_{eff}(V_{pp})$, due to material dispersion limitations, imperfect modal overlap factors with the active material, and low optical field strengths owing to the large diffraction-limited propagating waveguide mode area. Plasmonic devices clearly break off from the trend line deploying metal-insulator-metal (MIM) waveguide [25] or hybrid-plasmon-polaritons [8]. Their enhanced electric field strength (i.e., density of states) can be used to boost optical, classically weak, non-linear effects such as electro-optic modulation. This enhancement allows for the down-scaling of the device interaction length to a fraction of what diffraction-limited designs require. Hence, an interim conclusion is that high plasmonic waveguide losses are less of an issue than often stated. While some additional loss of plasmonic designs originate from the impedance mismatch between the diffraction-limited modes of the photonic circuit data-routing platform and the sub-diffraction limited plasmonic modes utilized for beam manipulation, the fact is that the total on-chip loss of plasmonic devices can actually dwarf that of non-plasmonic counterparts [5], [8].

With the apparent success of non-classical EOM design approaches, the remainder of the paper follows this guidance by investigating (a) EO potential of the transparent conductive oxide (TCO) ITO, and (b) a device design based on a plasmonic MOS-based waveguide as part of an SOI platform incorporating ITO as the active switching material.

3. Active Material Indium-Tin-Oxide Analysis

A key design choice of EO modulators is the material whose refractive index is actively modulated and the physical modulating mechanism i.e., Kerr Effect, the Franz-Keldysh effect and its quantum-confined version. Furthermore, shifting the Fermi Level [5] or the plasma frequency [5], [6] are promising effects that allow for the integration of emerging materials [5], [8], [9]. Ultimately, the combination of both modulation effect and material of the light-matter-interaction response is critical for efficiency and device performance. In this paper, we focus on an electrical carrier modulating effect in the active material Indium-Tin-Oxide (ITO) [40], [41]. ITO belongs to the family of conducting transparent oxides (TCO), which traditionally are deployed in the solar industry as low absorbing electrical contacts [42]. It has been shown that ITO can change its refractive index by unity upon charge accumulation in MOS-like structures in the visible frequency range [7]. In this section, we discuss how to estimate the ITO carrier concentration-based refractive index change that serves as a material input parameter in the device simulations below in a 2-step procedure; (a) determine the index for as-deposited ITO films, and (b) estimate the index change under voltage bias of a MOS-like device design.

Starting with the device ON-state, we deposited ITO films on a quartz substrate via physical vapor deposition, i.e., E-beam evaporation, and determined the resistivity via electrical 4-probe measurements. Given that typical ITO mobilities range from 10–40 cm^2/Vs, we assumed 15, which is a typical low-end value for the thin film deposition process used here [43]. The obtained carrier concentration, n_c, is then inserted into the Drude-Lorentz model. Note, this model has been previously used as transparent conductive oxides (TCO) like ITO [40], [41], and allows us to write the complex as

$$\varepsilon(\omega) = \varepsilon_\infty - \frac{\omega_p^2}{\omega(\omega + i\gamma)}; \quad \omega_p^2 = \frac{n_c e^2}{\varepsilon_0 m^*} \tag{5}$$

where γ is the electron scattering rate, ω is the angular momentum in rad/s, ε_0 and $\varepsilon_\infty = 1 + \chi = 3.9$ [44] are the free space and long-angular-momentum-limit permittivities, respectively, ω_p the plasma frequency, m^* the reduced mass of ITO equating to 0.35 m_0, with m_0 being the rest mass of the electron, n_c the voltage-modulated carrier density of the ITO film, and e the electron charge. Sweeping the free parameter, n_c, versus device operating frequency, we obtain the general function for the permittivity and index shown in Fig. 2.

If we assume an accumulation layer-induced carrier density increase inside the ITO, then the material should become more metallic, which increases the losses of the ITO film and hence that of the propagating MOS mode leading to an increased modal absorption. The electro-absorption modulation mechanism of the EOM device simulations below has its origin in this ITO loss modulating ability Fig. 2(d). In order to change the ITO material behavior from dielectric ($\varepsilon_1 > 1$, ε_2 small) to quasi metallic ($\varepsilon_1 \sim 1$, ε_2 larger) a carrier density of just below $n_c = 10^{21}$ cm^{-3} (arrow tip Fig. 2) is needed for an operating frequency of 228 THz (dashed vertical line in Fig. 2). The carrier density and hence the ITO's index change for the ON state (i.e., typically $V_b \sim 0$ V) was determined via 4-probe measurements. For the device OFF state (i.e., $V_b \neq 0$ V) we deployed a combination of both experimental measurements and analytical mode solvers to find the refractive indices of ITO [8]. The experimentally measured modal loss change $\Delta\kappa_m$ is 2.7% corresponding to a $\Delta\kappa_m/\Delta V_{bias} = 1\%\ V^{-1}$ [8]. Notice this is about 4 orders of magnitude larger as compared to diffraction-limited modulator designs [5], and highlights the plasmonic MOS mode enhanced modulation capability. Thus, we obtain the following refractive indices: $n_{ITO-ON} = 1.964 + i0.002$ and $n_{ITO-OFF} = 1.042 + i0.273$, which is a factor of 136 between the respective ON/OFF state extinction coefficients, κ. The change between these two indices is depicted by the black arrows, where the beginning and tip of the arrow indicate the carrier densities in the optical ON (light through) and OFF (light absorbed) state, respectively.

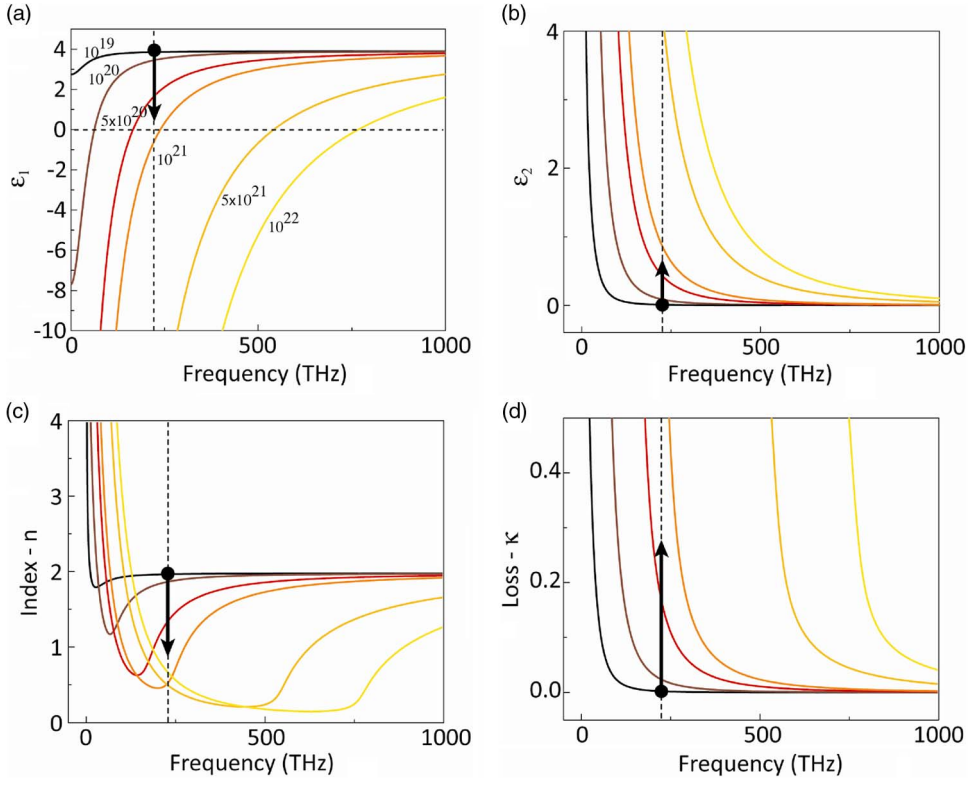

Fig. 2. Permittivity values from the Drude-Lorentz model for the ITO material versus frequency for various carrier densities (in units cm^{-3}). a and b are the real and imaginary parts of the permittivity, respectively, and c and d are the real and imaginary parts of the index of the ITO film. The black arrows highlight the carrier density change of the ITO as measured from film parameters and an analytical model. The start and tip of the arrow corresponds to the modulator ON and OFF state, respectively. Notice, how κ increases considerably from virtually zero to 0.273 in **d**. $\lambda = 1310$ nm vertical dashed line.

4. Device Design and Optical Modes

The electro-absorption modulator of this paper is based on a MOS design, which features deep sub-wavelength optical modes and reasonable long propagation lengths [45]–[50]. This optical mode is quite appropriate for densely integrated photonic on-chip components, 1) provides a strong light-matter-interaction resulting in (sub) λ-size active devices, 2) it allows to incorporate the device seamlessly into a low-loss SOI data-routing infrastructure, and 3) it smartly incorporates a metal contact which simultaneously serves as an electrical electrode and heat sink.

A schematic of the investigated devices is shown in Fig. 3. A variety of geometric parameters were used to optimize device performance; i.e., the Silicon oxide height of the capacitive gap (H_{SiO2}), the Silicon waveguide core thickness and width (H_{Si}, W_{Si}), the ITO height (H_{ITO}), and the length, L, of the device. The modulator's ER and IL performance originate and depend on the optical MOS mode, which is altered by changing the geometric parameters. A design-of-experiment parameter sweep is conducted in the next section below, but first we focus on the MOS mode under EOM device operation.

Using the values for the complex index of refraction of ITO from above, the MOS field distribution changes between the modulator absorbing OFF and light-through ON state (inset Fig. 3, numerical finite element solver (Comsol)). Unlike classical photonic modes, which display the strongest optical field density in the area with the highest refractive index, the plasmonic MOS deployed here shows its peak field (a) inside the gap between the metal and the semiconductor, and (b) in the lowest index region. The origin is discussed in [45]; briefly the continuity of the displacement field across the strong varying refractive index of this MOS mode stores optical energy inside the low-index gap

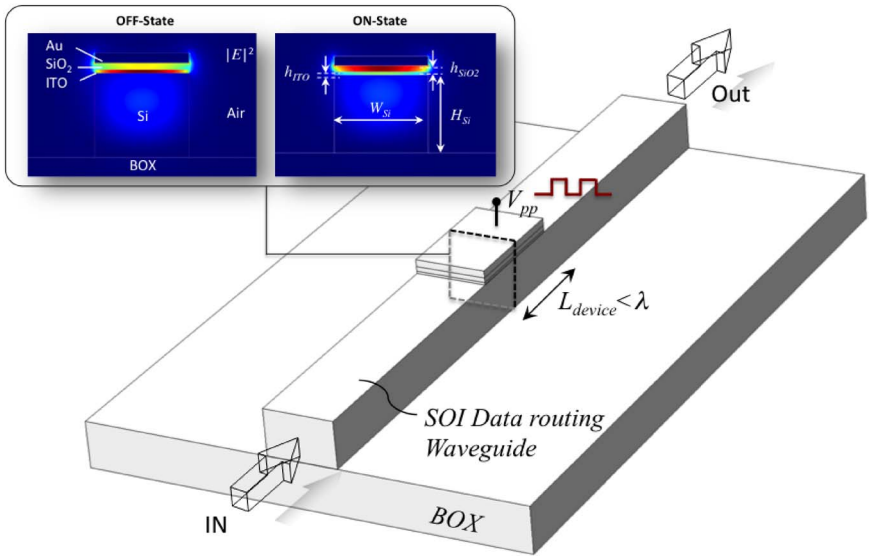

Fig. 3. Schematic of the sub-λ EO modulator. The active plasmonic modulation node can be placed arbitrarily placed into a SOI waveguide platform. The insets show the electric field densities for the OFF ($V_b = 4$ V, left) and ON-state ($V_b = 0$ V, right) state of the modulator, respectively. The peak of the electric field density is mainly concentrated in the silicon oxide gap in the ON-state and shifts to the strongly absorbing ITO layer in the OFF-state. Notice, the portion of the mode residing inside the Silicon core is desired and allows a small impedance mismatch between the MOS switching node and the SOI data routing backbone. Note, the electrical ground can be connected either to the Silicon waveguide or to the ITO. A commercial finite element analysis solver (Comsol) was used for the numerical simulations. $\lambda = 1310$ nm, material parameters: $\tilde{n}_{Si} = 3.541 - 0.0001i$, $\tilde{n}_{ITO-ON} = 1.964 - 0.002i$, $\tilde{n}_{ITO-OFF} = 1.042 - 0.273i$, $n_{SiO2} = 1.45$, $\tilde{n}_{Au} = 0.31 - 9.00i$.

region due to the creation of polarization charges. In the case here, this gap consists of two material layers, namely an oxide (here SiO_2), and the active material (here ITO). Using the real and imaginary parts for ITO from Fig. 2, one notices that the real part of the refractive index of ITO falls below and above that of SiO_2 for the modulator ON and OFF states, respectively. Thus, the peak optical field switches location between the gate-oxide and the active layer (inset Fig. 3). This is a desired effect, since it allows for a lower insertion loss in the ON state and a stronger modulation (i.e., higher ER) in the OFF state. For the latter, the strong optical loss of the metal-like ITO layer results in strong absorption. Note, the material choice for the top metal (here Gold) can be replaced by other materials such as Silver, Copper, or Aluminum if CMOS compatibility is desired. When changing the metal from Au to Al, the ER decreases by 9%, while IL increases by 17%. Comparing Gold to Copper, the ER increases by 5%, while IL also increases significantly by 372%. Note, while the lower modal loss for Al versus Cu appears counterintuitive at first, the plasmonic MOS modal loss does not entirely depend on the material losses, but more importantly of the field distribution; a lower κ_{metal} is a weaker optical capacitor than a higher κ_{metal}, and more optical field will therefore reside in the metal region resulting in an increased modal loss (i.e., Cu case) [45]. Thus, Aluminum appears to be the next best candidate for CMOS-critical designs.

5. EO Performance

In this section we analyze the EOM performance with respect to changes in the device geometry (Fig. 4). Rather than reporting on the extinction ratio, we decided to state the change in the effective extinction coefficient, $\Delta\kappa$, of the MOS mode as it is the physical change during the modulation process. Starting with altering the active material thickness (H_{ITO}), the modulation performance exhibits a maximum around an ITO thickness of 10 nm Fig. 4(a). This maximum is a result of two competing effects; in the long ITO gap limit, the index modulating carrier change inside the ITO is a result of the MOS capacitive charge accumulation layer altering the carrier density. The accumulation

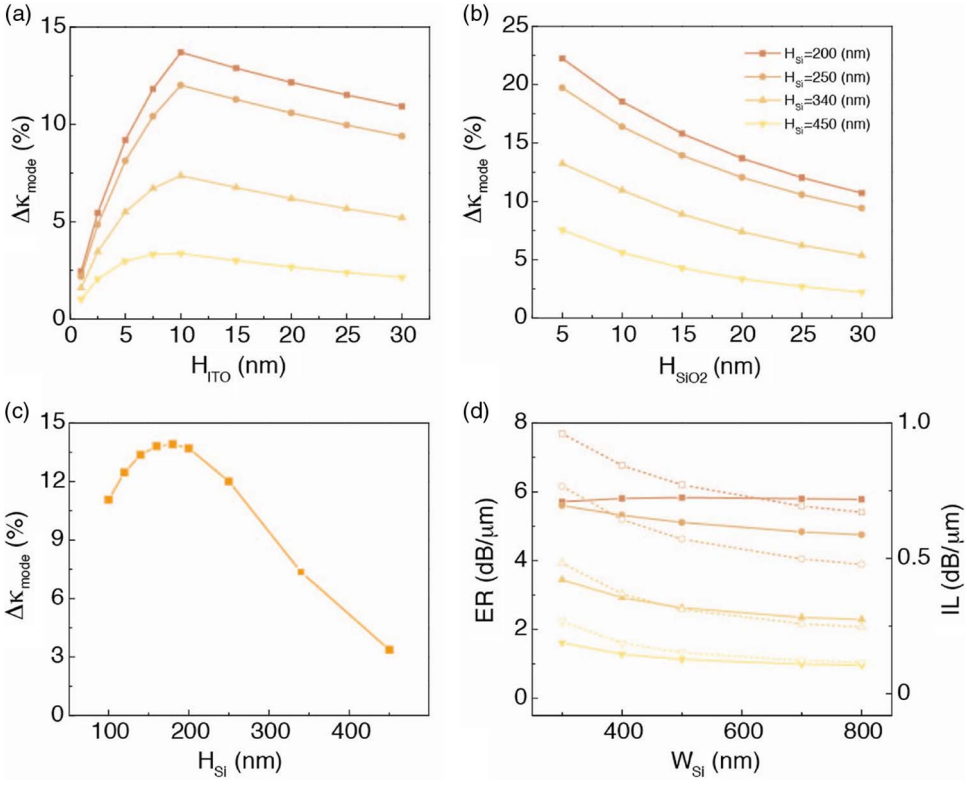

Fig. 4. Modulation performance for various geometrical device parameters. a–c, Change in the MOS mode's extinction coefficient versus ITO film thickness (a), versus MOS capacitor oxide gap height (b), and versus MOS stack Silicon core height (c). The different colors in a, b &d correspond to various Silicon core thicknesses and share the same legend. c, The optimum device Silicon core height is around 200 nm which is consistent with the highest optical confinement of the plasmonic MOS mode [45]. d, Optimized device performance, i.e., extinction ratio (ER, solid curves) and insertion loss (IL, dashed curves) versus device width (W_{Si}) and Silicon core height (H_{Si}). Note, these values are normalized to a device length of 0.78λ ($L_{device} = 1\ \mu$m) and highlight high performance (ER) of almost 6 dB with sub-1 dB on-chip insertion losses. $\lambda = 1310$ nm. The geometric parameters if not stated are $H_{ITO} = 10$ nm, $H_{SiO2} = 20$ nm, and $W_{Si} = 300$ nm.

layer thickness decreases exponentially with a $1/e$ depth of about 5 nm [7]. Thus, the refractive index of ITO is actually changing gradually as well. However, since a H_{ITO} of 10 nm was used to experimentally calibrate the index change [8], $\Delta\kappa$ in Fig. 4(a) is actually underestimated below $H_{ITO} = 10$ nm, and were overestimated above 10 nm if we would allow the entire ITO layer to be switched. Thus, we select a step-wise approximation by allowing for a complete index change for H_{ITO} up to 10 nm, and assume no index change for the remaining portion of the ITO layer larger than 10 nm. In addition, increasing the ITO thickness also loosens the optical confinement. Thus, the plasmonic light-matter-interaction enhancement will be damped with increased ITO thickness. In the low ITO gap limit, a total of three effects are present: 1) with decreasing gap the field enhancement increases, thus a raise of $\Delta\kappa$ would be expected [45]; 2) a smaller amount of the field resides in the enhanced region reducing the $\Delta\kappa$ of the effective mode; and 3) the field coupling coefficient between the ITO switched layer and the underlying Si layer is decreasing with reduced ITO gap sizes [45], [50]. All together explaining the long tail behavior. Noteworthy, previous studies on plasmonic MOS waveguides and lasers have resulted in similar optimized values of a gap of around 10 nm [46], [50]. The second observable of changing the ITO thickness is an enhanced modulation effect with decreasing Silicon core H_{Si} [see Fig. 4(a) and (c)]. This can be explained by a more plasmon-like behavior of the effective index of the mode, which pushes more field into the gap with decreasing silicon core height. This is consistent with the original findings of the plasmonic MOS mode

reported by Oulton *et al.* [45]. However, for extremely thin silicon cores, the optical confinement loosens quickly, and results in reduced modulation [see Fig. 4(c)] [45]. The Silicon core thickness for optimum modulation performance is found to be around 200 nm and, scales, in general, with the core index [45].

Another geometrical parameter is the MOS capacitor oxide gap, which controls the electrostatics of the ITO accumulation layer. Decreasing this oxide (here SiO_2) thickness leads to a stronger electric field inside the device resulting in a higher index carrier density and hence an index change in the ITO; see Fig. 4(b). Decreasing the H_{SiO2} from 30 to 5 nm results in a 2x increase in the modulation performance. Similar to Fig. 4(a) and (c), decreasing H_{Si} improves the modulation behavior by almost one order of magnitude.

Scaling down the device length of the modulator is important for both realizing a low insertion loss and high operating speed, i.e., low electrical capacitance. Low IL is a general challenge for plasmonic-based modulators due to the inherent SPP loss of the mode. However, for ultra-compact (i.e., sub-λ long) device lengths, IL can be quite low, and the design task is to ensure sufficient ER for logic operations above the signal-to-noise level of the photodetector. In order to test the device performance of a sub-λ long plasmonic EOM device, we simulated the performance (i.e., ER & IL) of a 0.78λ long device, shown in Fig. 4(d). Here, we select the optimized parameters from Fig. 4(a) and (b), and sweep the only free geometric parameter, that is the Silicon width, H_{Si}, (i.e., MOS stack width). The general trend for ER is to increase strongly with decreasing Silicon height and to increase gradually with decreasing the MOS stack width. The insertion loss, which is a function of κ_{ON}, scales similarly as the extinction ratio due to the same field confinement arguments above. However, an exception is the case for $H_{Si} = 200$ nm; here ER is rather flat with W_{Si} [see Fig. 4(d): orange solid line]. The reason for this is that the portion of the optical energy residing in the Silicon core is close to being cut-off, which happens around 218 nm $(\lambda/2n_{eff} = 218\ \text{nm}, n_{eff} = 3.0, \lambda = 1310\ \text{nm})$. Thus, this denotes an optimum modulation case where most of the energy of the mode is pushed into the MOS gap, increasing the ITO-mode overlap factor. Interestingly, while ER is flat for this case, the insertion loss does change with H_{Si}. The reason for this is that the amount of optical energy in the gap region of this plasmonic MOS mode is increasing due to the lateral confinement effect. Commenting on the overall performance of the device, the highest extinction ratio is about 6 dB/μm, which is quite outstanding. At the same time, this high modulation performance is accompanied by a reasonably low insertion loss of 0.7 dB.

6. Conclusion

In this paper, we have demonstrated an ultra-compact electro-absorption modulator (EOM) based on a plasmonic MOS-mode design. Different EOM performances have been achieved with respect to changes in the device geometry. In our simulation, 6 dB/μm high extinction ratio with a low insertion loss of 0.7 dB has been shown for 0.78λ long device. Furthermore, benchmarking EOM device performance results in plasmonic devices displaying a significant performance potential beyond that of classical (i.e., diffraction-limited) architectures. With respect to the potential for future communication networks and computing, highly scalable EOMs that feature strong modulation performance and low power consumption will allow for advancements in network communication and computing speed.

Acknowledgment

We thank Dr. Salandrino and C. Ye for helpful discussions.

References

[1] M. Haurylau, G. Chen, H. Chen, J. Zhang, N. A. Nelson, D. H. Albonesi, E. G. Friedman, and P. M. Fauchet, "On-chip optical interconnect roadmap: Challenges and critical directions," *IEEE J. Sel. Topics Quantum Electron.*, vol. 12, no. 6, pp. 1699–1705, Nov./Dec. 2006.

[2] J. Rattner, "The future of silicon photonics," presented at the Proc. IPRSN, Monterey, CA, USA, 2010, JTuA1.

[3] D. F. Welch, F. A. Kish, R. Nagarajan, C. H. Joyner, R. P. Schneider, V. G. Dominic, M. L. Mitchell, S. G. Grubb, T.-K. Chiang, D. D. Perkins, and A. C. Nilsson, "The realization of large-scale photonic integrated circuits and the associated impact on fiber-optic communication systems," *J. Lightw. Technol.*, vol. 24, no. 12, pp. 4674–4683, Dec. 2006.
[4] J. Liu, D. Pan, S. Jongthammanurak, S. Jongthammanurak, K. Wada, L. C. Kimerling, and J. Michel, "Design of monolithically integrated GeSi electroabsorption modulators and photodetectors on an SOI platform," *Opt. Exp.*, vol. 15, no. 2, pp. 623–628, Jan. 2007.
[5] M. Liu, X. Yin, E. Ulin-Avila, B. Geng, T. Zentgraf, L. Ju, F. Wang, and X. Zhang, "A graphene-based broadband optical modulator," *Nature*, vol. 474, no. 7349, pp. 64–67, Jun. 2011.
[6] Q. Xu, B. Schmidt, S. Pradhan, and M. Lipson, "Micrometre-scale silicon electro-optic modulator," *Nature*, vol. 435, no. 7040, pp. 325–327, May 2005.
[7] E. Feigenbaum, K. Diest, and H. A. Atwater, "Unity-order index change in transparent conducting oxides at visible frequencies," *Nano Lett.*, vol. 10, no. 6, pp. 2111–2116, Jun. 2010.
[8] V. J. Sorger, D. Kimura, R.-M. Ma, and X. Zhang, "Ultra-compact silicon nanophotonic modulator with broadband response," *Nanophotonics*, vol. 1, no. 1, pp. 17–22, Jul. 2012.
[9] Z. Lu and W. Zhao, "Nanoscale electro-optic modulators based on graphene-slot waveguides," *J. Opt. Soc. Amer. B, Opt. Phys.*, vol. 29, no. 6, pp. 1490–1496, Jun. 2012.
[10] W. Cai, J. S. White, and M. L. Brongersma, "Compact, high-speed and power-efficient electrooptic plasmonic modulators," *Nano Lett.*, vol. 9, no. 12, pp. 4403–4411, Dec. 2009.
[11] A. V. Krasavin and A. V. Zayats, "Photonic signal processing on electronic scales: Electro-optical field-effect nanoplasmonic modulator," *Phys. Rev. Lett.*, vol. 109, no. 5, pp. 053901-1–053901-5, Jul. 2012.
[12] J. A. Dionne, K. Diest, L. A. Sweatlock, and H. A. Atwater, "PlasMOStor: A metal-oxide-Si field effect plasmonic modulator," *Nano Lett.*, vol. 9, no. 2, pp. 897–902, Feb. 2009.
[13] H. Lin, O. Ogbuu, J. Liu, L. Zhang, J. Michel, and J. Hu, "Breaking the energy-bandwidth limit of electro-optic modulators: Theory and a device proposal," presented at the Proc. CLEO, Sci. Innov., San Jose, CA, USA, 2013, CTu3J.7.
[14] S. A. Maier, *Plasmonics, Fundamentals and Applications*. New York, NY, USA: Springer-Verlag, 2007.
[15] S. Ren, Y. Rong, S. A. Claussen, R. K. Schaevitz, T. I. Kamins, S. James, and D. A. B. Miller, "Ge/SiGe quantum well waveguide modulator monolithically integrated with SOI waveguides," *IEEE Photon. Technol. Lett.*, vol. 24, pp. 461–463, Mar. 2012.
[16] N. Feng, D. Feng, S. Liao, X. Wang, P. Dong, H. Liang, C.-C. Kung, W. Qian, J. Fong, R. Shafiiha, Y. Luo, J. Cunningham, A. V. Krishnamoorthy, and M. Asghari, "30 GHz Ge electro-absorption modulator integrated with 3 μm silicon-on-insulator waveguide," *Opt. Exp.*, vol. 19, no. 8, pp. 7062–7067, Apr. 2011.
[17] Y. Tang, H. Chen, S. Jain, J. D Peters, U. Westergren, and J. E. Bowers, "50 Gb/s hybrid silicon traveling-wave electroabsorption modulator," *Opt. Exp.*, vol. 19, no. 7, pp. 5811–5816, Mar. 2011.
[18] Y. Kuo, H. Chen, and J. E. Bowers, "High speed hybrid silicon evanescent electroabsorption modulator," *Opt. Exp.*, vol. 16, no. 13, pp. 9936–9941, Jun. 2008.
[19] H. Fukano, T. Yamanaka, M. Tamura, and Y. Kondo, "Very-low-driving-voltage electroabsorption modulators operating at 40 Gb/s," *J. Lightw. Technol.*, vol. 24, no. 5, pp. 2219–2224, May 2006.
[20] M. Chacinski, U. Westergren, B. Willen, B. Stoltz, and L. Thylen, "Electro absorption modulators suitable for 100-Gb/s Ethernet," *IEEE Electron Device Lett.*, vol. 29, no. 9, pp. 1014–1016, Sep. 2008.
[21] D. Feng, S. Liao, H. Liang, J. Fong, B. Bijlani, R. Shafiiha, B. J. Luff, Y. Luo, J. Cunningham, A. V. Krishnamoorthy, and M. Asghari, "High speed GeSi electro-absorption modulator at 1550 nm wavelength on SOI waveguide," *Opt. Exp.*, vol. 20, no. 20, pp. 22 224–22 232, Sep. 2012.
[22] J. Liu, M. Beals, A. Pomerene, S. Bernardis, R. Sun, J. Cheng, L. C. Kimerling, and J. Michel, "Ultralow energy, integrated GeSi electroabsorption modulators on SOI," in *Proc. 5th IEEE Int. Conf. Group IV Photon.*, 2008, pp. 10–12.
[23] S. Irmscher, R. Lewen, and U. Eriksson, "InP–InGaAsP high-speed traveling-wave electroabsorption modulators with integrated termination resistors," *IEEE Photon. Technol. Lett.*, vol. 14, no. 7, pp. 923–925, Jul. 2002.
[24] A. Melikyan, N. Lindenmann, S. Walheim, P. M. Leufke, S. Ulrich, J. Ye, P. Vincze, H. Hahn, Th. Schimmel, C. Koos, W. Freude, and J. Leuthold, "Surface plasmon polariton absorption modulator," *Opt. Exp.*, vol. 19, no. 9, pp. 8855–8869, Apr. 2011.
[25] S. Zhu, G. Q. Lo, and D. L. Kwong, "Electro-absorption modulation in horizontal metal-insulator-silicon-insulator metal nanoplasmonic slot waveguides," *Appl. Phys. Lett.*, vol. 99, no. 15, pp. 151114-1–151114-3, Oct. 2011.
[26] F. Devaux, F. Dorgeuille, A. Ougazzaden, F. Huet, M. Carre, A. Carenco, M. Henry, Y. Sorel, J.-F. Kerdiles, and E. Jeanney, "20 Gbit/s operation of a high-efficiency InGaAsP/InGaAsP MQW electroabsorption modulator with 1.2 V drive voltage," *IEEE Photon. Technol. Lett.*, vol. 5, no. 11, pp. 1288–1290, Nov. 1993.
[27] Y.-J. Chiu, H. Chou, V. Kaman, P. Abraham, and J. E. Bowers, "High extinction ratio and saturation power traveling-wave electroabsorption modulator," *IEEE Photon. Technol. Lett.*, vol. 14, no. 6, pp. 792–794, Jun. 2002.
[28] J.-W. Shi, A.-C. Shiao, C.-C. Chu, and Y.-S. Wu, "Dual-depletion-region electroabsorption modulator with evanescently coupled waveguide for high-speed ($>$ 40 GHz) and low driving-voltage performance," *IEEE Photon. Technol. Lett.*, vol. 19, no. 5, pp. 345–347, Mar. 2007.
[29] M. Tamura, T. Yamanaka, H. Fukano, Y. Akage, Y. Kondo, and T. Saitoh, "High-speed electroabsorption modulators buried with ruthenium-doped SI-InP," *IEEE Photon. Technol. Lett.*, vol. 16, no. 12, pp. 2613–2615, Dec. 2004.
[30] K. Satzke, D. Baums, U. Cebulla, H. Haisch, D. Kaiser, E. Lach, E. Kuhn, J. Weber, R. Weinmann, P. Wiedemann, and E. Zielinski, "Ultrahigh-bandwidth (42 GHz) polarization-independent ridge waveguide electroabsorption modulator based on tensile strained InGaAsP MQW," *Electron. Lett.*, vol. 31, no. 23, pp. 2030–2032, Nov. 1995.
[31] O. Qasaimeh, P. Bhattacharya, and E. T. Croke, "SiGe–Si quantum-well electroabsorption modulators," *IEEE Photon. Technol. Lett.*, vol. 10, no. 6, pp. 807–809, Jun. 1998.
[32] S. Z. Zhang, Y.-J. Chiu, P. Abraham, and J. E. Bowers, "25-GHz polarization-insensitive electroabsorption modulators with traveling-wave electrodes," *IEEE Photon. Technol. Lett.*, vol. 11, no. 2, pp. 191–193, Feb. 1999.

[33] H. Tada, Y. Miyazaki, K. Takagi, T. Aoyagi, T. Nishimura, and E. Omura, "40 GHz modulation bandwidth of electro-absorption modulator with narrow-mesa ridge waveguide," in *Proc. Opt. Fiber Commun. Conf. Exhib.*, 2002, pp. 722–723.
[34] K. J. A. Ooi, P. Bai, S. C. Hong, and L. K. Ang, "Ultracompact vanadium dioxide dual-mode plasmonic waveguide electroabsorption modulator," *Nanophotonics*, vol. 2, no. 1, pp. 13–19, Feb. 2013.
[35] T. Ido, S. Tanaka, M. Suzuki, M. Koizumi, H. Sano, and H. Inoue, "Ultra-high-speed multiple-quantum-well electro-absorption optical modulators with integrated waveguides," *J. Lightw. Technol.*, vol. 14, no. 9, pp. 2026–2034, Sep. 1996.
[36] A. E. Bond, G. Shtengel, Y. Akulova, and C. L. Reynolds, Jr., *43 GHz modulation bandwidth packaged InGaAsP MQW EA modulators with integrated mode converters*, Lucent Technologies.
[37] Y.-J. Chiu, S. Z. Zhang, K. Volkan, J. Piprek, and J. E. Bowers, "High-speed traveling-wave electroabsorption modulators," in *Proc. SPIE*, San Diego, CA, USA, 2001, vol. 4490, pp. 1–10.
[38] M. Liu, X. Yin, and X. Zhang, "Double-layer graphene optical modulator," *Nano Lett.*, vol. 12, no. 3, pp. 1482–1485, Mar. 2012.
[39] S. J. Koester and M. Li, "High-speed waveguide-coupled graphene-on-graphene optical modulators," *Appl. Phys. Lett.*, vol. 100, no. 17, pp. 171107-1–171107-4, Apr. 2012.
[40] R. G. Gordon, "Criteria for choosing transparent conductors," *MRS Bull.*, vol. 25, no. 8, pp. 52–57, Aug. 2000.
[41] I. Hamberg and C. G. Granqvist, "Evaporated Sn-doped In_2O_3 films: Basic optical properties and applications to energy-efficient windows," *J. Appl. Phys.*, vol. 60, no. 11, pp. R123–R159, Dec. 1986.
[42] G. Giusti, "Deposition and characterisation of functional ITO thin," Ph.D. dissertations, School Metall. Mater., Univ. of Birmingham, Birmingham, U.K., 2011.
[43] F. Kurdesau, G. Khripunov, A. F. da Cunha, M. Kaelin, and A. N. Tiwarid, "Comparative study of ITO layers deposited by DC and RF magnetron sputtering at room temperature," *J. Non-Cryst. Solids*, vol. 352, no. 9–20, pp. 1466–1470, Jun. 2006.
[44] F. Michelotti, L. Dominici, E. Descrovi, N. Danz, and F. Menchini, "Thickness dependence of surface plasmon polariton dispersion in transparent conducting oxide films at 1.55 mm," *Opt. Lett.*, vol. 34, no. 6, pp. 839–841, Mar. 2009.
[45] R. F. Oulton, V. J. Sorger, D. F. B. Pile, D. Genov, and X. Zhang, "A hybrid plasmonic waveguide for subwavelength confinement and long-range propagation," *Nature Photon.*, vol. 2, no. 8, pp. 496–500, Aug. 2008.
[46] R. F. Oulton, V. J. Sorger, T. Zentgraf, R. M. Ma, C. Gladden, L. Dai, G. Bartal, and X. Zhang, "Plasmon lasers at deep subwavelength scale," *Nature*, vol. 461, no. 7264, pp. 629–632, Oct. 2009.
[47] V. J. Sorger, Z. Ye, R. F. Oulton, G. Bartal, Y. Wang, and X. Zhang, "Experimental demonstration of low-loss optical waveguiding at deep sub-wavelength scales," *Nature Commun.*, vol. 2, no. 5, p. 331, May 2011.
[48] V. J. Sorger and X. Zhang, "A spotlight on plasmon lasers," *Science*, vol. 333, no. 6043, pp. 709–710, Aug. 2011.
[49] R. M. Ma, R. F. Oulton, V. J. Sorger, G. Bartal, and X. Zhang, "Room-temperature sub-diffraction-limited plasmon laser by total internal reflection," *Nature Mater.*, vol. 10, no. 2, pp. 110–113, Feb. 2011.
[50] V. J. Sorger, N. Pholchai, E. Cubukcu, R. F. Oulton, P. Kolchin, C. Borschel, M. Gnauck, C. Ronning, and X. Zhang, "Strongly enhanced molecular fluorescence inside a nanoscale waveguide gap," *Nano Lett.*, vol. 11, no. 11, pp. 4907–4911, Nov. 2011.